



 Cite this: *RSC Adv.*, 2023, **13**, 34510

# High-efficiency energy transfer in the strong orange-red-emitting phosphor $\text{CeO}_2:\text{Sm}^{3+}$ , $\text{Eu}^{3+}$

 Nguyen Van Hai,<sup>a</sup> Nguyen Thi Khanh Linh,<sup>a</sup> Dinh Thi Hien,<sup>a</sup> Bui Thi Hoan,<sup>b</sup> Nguyen Minh Tu,<sup>c</sup> Vuong-Hung Pham,<sup>d</sup> Duy-Hung Nguyen,<sup>d</sup> Vu Tuan Anh<sup>e</sup> and Hoang Nhu Van \*<sup>e</sup>

High-efficiency energy transfer (ET) from  $\text{Sm}^{3+}$  to  $\text{Eu}^{3+}$  leads to dominant red emission in  $\text{Sm}^{3+}$ ,  $\text{Eu}^{3+}$  co-doped single-phase cubic  $\text{CeO}_2$  phosphors. In this work, a series of  $\text{Sm}^{3+}$  singly and  $\text{Sm}^{3+}/\text{Eu}^{3+}$  co-doped  $\text{CeO}_2$  cubic phosphors was successfully synthesized by solution combustion followed by heat treatment at 800 °C in air. The crystal structure, morphology, chemical element composition, and luminescence properties of the obtained phosphors were investigated using X-ray diffraction, scanning electron microscopy, energy-dispersive X-ray spectroscopy, and photoluminescence analysis. Under 360 nm excitation, the  $\text{Sm}^{3+}$  singly doped  $\text{CeO}_2$  phosphor emitted strong yellow-red light at 573 nm ( $^4\text{G}_{5/2}-^6\text{H}_{5/2}$ ) and 615 nm ( $^4\text{G}_{5/2}-^6\text{H}_{7/2}$ ). Meanwhile, the  $\text{CeO}_2:\text{Sm}^{3+}$ ,  $\text{Eu}^{3+}$  phosphors showed the emission characteristic of both  $\text{Sm}^{3+}$  and  $\text{Eu}^{3+}$ , with the highest emission intensity at 631 nm. The emission intensity of  $\text{Sm}^{3+}$  decreased with increasing  $\text{Eu}^{3+}$  content, suggesting the ET from  $\text{Sm}^{3+}$  to  $\text{Eu}^{3+}$  in the  $\text{CeO}_2:\text{Sm}^{3+}$ ,  $\text{Eu}^{3+}$  phosphors. The decay kinetics of the  $^4\text{G}_{5/2}-^6\text{H}_{5/2}$  transition of  $\text{Sm}^{3+}$  in the  $\text{CeO}_2:\text{Sm}^{3+}$ ,  $\text{Eu}^{3+}$  phosphors were investigated, confirming the high-efficiency ET from  $\text{Sm}^{3+}$  to  $\text{Eu}^{3+}$  (reached 84%). The critical distance of energy transfer ( $R_C = 13.7$  Å) and the Dexter theory analysis confirmed the ET mechanism corresponding to the quadrupole–quadrupole interaction. These results indicate that the high-efficiency ET from  $\text{Sm}^{3+}$  to  $\text{Eu}^{3+}$  in  $\text{CeO}_2:\text{Sm}^{3+}$ ,  $\text{Eu}^{3+}$  phosphors is an excellent strategy to improve the emission efficiency of  $\text{Eu}^{3+}$ .

 Received 6th November 2023  
 Accepted 17th November 2023

DOI: 10.1039/d3ra07567b

[rsc.li/rsc-advances](http://rsc.li/rsc-advances)

## 1. Introduction

White-light emitting diodes (WLEDs) have been extensively used in many fields of application, such as in solid lighting, display devices, and optoelectronic devices, because of their high luminous efficiency, long lifetime, energy saving, and environment friendliness.<sup>1–3</sup> A popular method for manufacturing WLEDs is combining tricolor phosphor powder (blue, green, and red phosphors) with an ultraviolet (UV) InGaN chip.<sup>4,5</sup> However, these WLEDs present a high correlated color temperature and low color rendering index due to the lack of a red component.<sup>6,7</sup> To overcome these drawbacks, scholars should explore new red phosphors for WLED applications.

The europium trivalent ion ( $\text{Eu}^{3+}$ ) is an important rare-earth (RE) ion that has been widely used as an activator in red-emitting phosphors for WLEDs.<sup>8–10</sup> The red emission of  $\text{Eu}^{3+}$  is originally from electric dipole transitions. Notably,  $\text{Eu}^{3+}$ -doped phosphors typically exhibit relatively narrow absorption in UV and near-UV regions because of the spin-forbidden transition of  $\text{Eu}^{3+}$ , resulting in low emission efficiency.<sup>11,12</sup> This defect can be compensated by introducing sensitizing ions, such as  $\text{Tb}^{3+}$ ,  $\text{Bi}^{3+}$ ,  $\text{Gd}^{3+}$ , and  $\text{Sm}^{3+}$ ,<sup>13–15</sup> which can absorb excitation energy efficiently and transfer it to  $\text{Eu}^{3+}$ .  $\text{Sm}^{3+}$  is a popular sensitizer for improving the efficiency emission of  $\text{Eu}^{3+}$  ion due to the small energy difference between the  $^4\text{G}_{5/2}$  level of  $\text{Sm}^{3+}$  and the  $^5\text{D}_0$  level of  $\text{Eu}^{3+}$  (about 600  $\text{cm}^{-1}$ ), leading to easy phonon-assisted energy transfer (ET).<sup>13</sup> Hence, the energy transfer between  $\text{Sm}^{3+}$  and  $\text{Eu}^{3+}$  ions was widely investigated in a variety of host lattices.<sup>12,16,17</sup> J. Wu *et al.*<sup>16</sup> found that the ET efficiency from  $\text{Sm}^{3+}$  to  $\text{Eu}^{3+}$  up to 65% in  $\text{YPO}_4:\text{Sm}^{3+}$ ,  $\text{Eu}^{3+}$  phosphor corresponds to the electric dipole–electric dipole interaction mechanism. Y. Li *et al.*<sup>17</sup> reported that ET efficiency from  $\text{Sm}^{3+}$  to  $\text{Eu}^{3+}$  was 13.7% in  $\text{La}_2\text{CaB}_{10}\text{O}_{19}:\text{Sm}^{3+}$ ,  $\text{Eu}^{3+}$  phosphor, further confirmed by Judd–Ofelt theory. Meanwhile, X. Zhang *et al.*<sup>12</sup> developed  $\text{Ca}_2\text{GdNbO}_6:\text{Sm}^{3+}$ ,  $\text{Eu}^{3+}$  phosphor with high quantum yield (82.7%), excellent thermal stability, and up to 28.6% ET efficiency. In addition, the LED device fabricated

<sup>a</sup>Faculty of Chemistry, Hanoi National University of Education, 136 Xuan Thuy Road, Cau Giay District, Hanoi, Viet Nam

<sup>b</sup>Faculty of Electrical–Electronics Engineering, Thuyloi University, No. 175 Tay Son Road, Hanoi, Viet Nam

<sup>c</sup>Faculty of Pharmacy, Phenikaa University, Yen Nghia, Ha-Dong District, Hanoi 12116, Viet Nam

<sup>d</sup>International Training Institute for Materials Science (ITIMS), Hanoi University of Science and Technology, No. 01, Dai Co Viet Road, Ha Noi, Viet Nam

<sup>e</sup>Faculty of Materials Science and Engineering, Phenikaa University, Yen Nghia, Ha-Dong District, Hanoi 12116, Viet Nam. E-mail: van.hoangnhu@phenikaa-uni.edu.vn


based on this phosphor emits bright white light, and CCT = 5400 K,  $R_a = 92.8$ . Clearly, the addition of two or more RE ions into a luminescent material can effectively control multi-color luminescence and achieve ET, thereby improving the luminous efficiency of the phosphors.<sup>7,11,13,18</sup> Besides, several parameters, including the degree of crystallinity, the dopant concentration, and the host material, influence the emission efficiency of the phosphors. In this case, the host lattice selection is important since it influences the luminescent efficiency and the application potential of the material.

Cerium oxide (CeO<sub>2</sub>) host lattice exhibits low phonon energy, high thermal stability, low toxicity, and excellent physico-chemical properties.<sup>19–21</sup> It is an attractive UV-excited host material due to its strong light absorption through the O<sup>2–</sup>–Ce<sup>4+</sup> charge transfer band. Therefore, RE-doped CeO<sub>2</sub> was widely investigated for many applications, such as catalysis, sensors, optoelectronic devices, and UV-LEDs.<sup>20,22</sup> The small difference between the ionic radius of Ce<sup>4+</sup> and RE<sup>3+</sup> suggests that it can provide favorable sites for introducing RE ions into the CeO<sub>2</sub> host lattice. Furthermore, the spectral overlap of the CeO<sub>2</sub> host's charge transfer band and the 4f–4f transitions of the RE ions leads to highly efficient energy transfer from host to RE ions.<sup>23,24</sup> G. Vimal *et al.*<sup>23</sup> have observed the energy transfer from the CeO<sub>2</sub> host to Eu<sup>3+</sup> in CeO<sub>2</sub>:Sm<sup>3+</sup>, Eu<sup>3+</sup> phosphor leading to improved efficiency emission of the systems. Meanwhile, an intense red emission of Eu<sup>3+</sup> was achieved in CeO<sub>2</sub>:Eu<sup>3+</sup>, Bi<sup>3+</sup>,<sup>24</sup> and CeO<sub>2</sub>:Eu<sup>3+</sup>, M<sup>+</sup> (M: Na, K, Li)<sup>25</sup> phosphors through change the symmetry of the host and charge compensation mechanism, respectively. However, achieving a high-efficiency energy transfer in orange-red-emitting phosphor CeO<sub>2</sub>:Sm<sup>3+</sup>, Eu<sup>3+</sup> synthesized by solution combustion and its energy transfer mechanism investigation have not been well documented.

In this work, a series of Sm<sup>3+</sup> singly and Sm<sup>3+</sup>/Eu<sup>3+</sup> co-doped CeO<sub>2</sub> phosphors was prepared using solution combustion method. The crystal structure and chemical element composition were explored using X-ray diffraction and energy-dispersive X-ray spectroscopy analyses. The luminescence properties and ET mechanisms were systematically investigated. The phosphors emitted orange to red emissions with an enhancement of Eu<sup>3+</sup> doping because the efficiency of ET from Sm<sup>3+</sup> to Eu<sup>3+</sup> reached 84%. Furthermore, the ET mechanism between Sm<sup>3+</sup> and Eu<sup>3+</sup> was discussed in detail.

## 2. Experimental procedure

A series of CeO<sub>2</sub>:*x*Sm<sup>3+</sup> (*x* = 0.02, 0.04, 0.06, 0.08, 0.10, and 0.12 mol%), CeO<sub>2</sub>:0.04Eu, and CeO<sub>2</sub>:0.04Sm<sup>3+</sup>, *y*Eu<sup>3+</sup> (*y* = 0, 0.02, 0.04, 0.06, 0.08, and 0.10 mol%) phosphors was prepared using solution combustion followed by heat treatment at 800 °C for 4 h in air. Ce(NO<sub>3</sub>)<sub>3</sub>·6H<sub>2</sub>O (Sigma-Aldrich, 99.9%), Sm(NO<sub>3</sub>)<sub>3</sub>·6H<sub>2</sub>O (Sigma-Aldrich, 99.99%), urea, and Eu<sub>2</sub>O<sub>3</sub> (Sigma-Aldrich, 99.99%) were used as raw materials. These materials were exactly weighed and dissolved in deionized water and HNO<sub>3</sub> solution (Eu<sub>2</sub>O<sub>3</sub>) under magnet-stirred conditions to obtain aqueous solutions Ce<sup>3+</sup> (0.5 M), Sm<sup>3+</sup> (0.5 M), and Eu<sup>3+</sup> (0.5 M), respectively. The stoichiometric amounts of the solutions Ce<sup>3+</sup>, Sm<sup>3+</sup>, and Eu<sup>3+</sup> were added together to get 0.5 M aqueous solution and stirred for

30 min at room temperature. After that, the 20 mol% urea (compared with the Ce<sup>3+</sup> content) was added to the system under magnetic stirring for 3 h at 80 °C. Next, the system was transferred to a corundum crucible (200 ml) for combustion reaction at 400 °C for 4 h. Then, the powder was heat-treated at 800 °C for 4 h in air, with a heating rate of 3 °C per minute. Finally, obtained phosphor powder was naturally cooled to room temperature and characterized. The crystal structure and chemical element composition of the phosphors were determined by X-ray diffraction (Bruker D8 Advance) and energy-dispersive X-ray spectroscopy (JEM 1010, JEOL Technique, Tokyo, Japan) analyses. The luminescence properties, lifetime, and ET mechanisms were investigated using a NANOLOG spectrophotometer (Horiba, USA). Decay curves of the investigated phosphors were also evaluated.

## 3. Results and discussion

### 3.1. XRD analysis

Fig. 1a presents the XRD patterns of CeO<sub>2</sub>:0.04Sm<sup>3+</sup> phosphors without and co-doped with Eu<sup>3+</sup>. All the diffraction peaks are consistent with the standard card (PDF # 01-075-8371), confirming the formation of single-phase cubic fluorite-type CeO<sub>2</sub> with space group *Fm3m* and no impurity phase is present. The crystal structure of CeO<sub>2</sub> includes Ce<sup>4+</sup> sites with eight coordinates (including eight nearest-neighbor oxygen anions) and O<sup>2–</sup> sites with four coordinates (surrounded by four nearest-neighbor cerium cations).<sup>26</sup> High-intensity diffraction peaks were observed corresponding to typical planes of cubic phase CeO<sub>2</sub> including (111), (200), (220), (311), (222), and (400). Significantly, the diffraction peaks shifted toward a lower  $2\theta$  angle (Fig. 1b) after being doped with a larger ionic radius Eu<sup>3+</sup> (1.06 Å) since the ionic radius of Ce<sup>4+</sup> is 0.97 Å, leading to a lattice expansion,<sup>18</sup> confirming that Eu<sup>3+</sup> ions have been incorporated in the Ce<sup>4+</sup> sites of the CeO<sub>2</sub> host. Furthermore, the crystallite size of all investigated phosphors was determined using the Scherrer equation:<sup>27</sup>

$$D = \frac{0.9\lambda}{\beta \cos(\theta)} \quad (1)$$

where *D* is crystallite size (nm), 0.9 is Scherrer constant,  $\lambda$  is the wavelength of the X-ray sources (0.15406 nm),  $\beta$  (radians) and  $\theta$  (radians) are full width at half maximum (FWHM) and peak position, respectively. The diffraction peak corresponding to the (111) plane of CeO<sub>2</sub> was chosen to calculate crystallite size, as shown in Table 1. Notably, the crystallite size slightly increases with increasing Eu<sup>3+</sup> doping, suggesting a successful introduction of Eu<sup>3+</sup> in the systems. These results confirm that the presence of Eu<sup>3+</sup> in the systems leads to enhanced crystallinity and crystallite size, which could improve the emission efficiency of the phosphors.

### 3.2. Morphology and chemical element composition analysis

Fig. 2a and b show the SEM images of CeO<sub>2</sub>:0.04Sm<sup>3+</sup> and CeO<sub>2</sub>:0.04Sm<sup>3+</sup>, 0.04Eu<sup>3+</sup>, respectively. The un-doped sample (CeO<sub>2</sub>:0.04Sm<sup>3+</sup>) shows the agglomeration of spherical-like



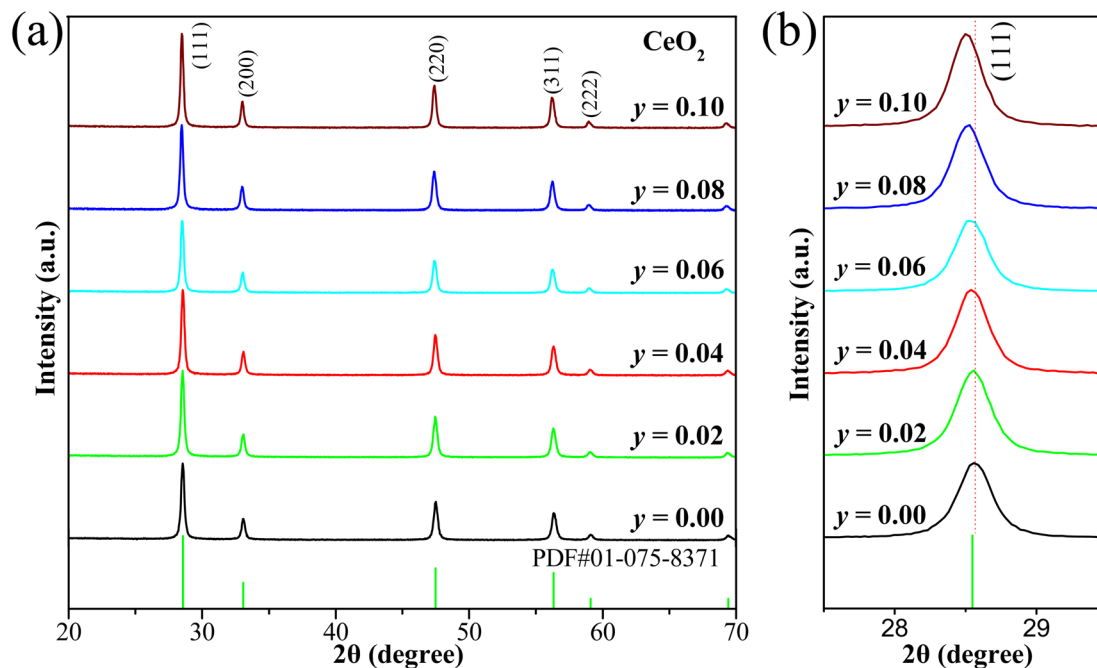


Fig. 1 (a) XRD patterns of the investigated samples  $\text{CeO}_2:0.04\text{Sm}^{3+}, y\text{Eu}^{3+}$  ( $y = 0.00, 0.02, 0.04, 0.06, 0.08,$  and  $0.10$ ), and (b) XRD patterns at  $2\theta$  angle of  $27.5^\circ$  to  $29.5^\circ$  of all samples.

Table 1 The crystallite size of samples with different  $\text{Eu}^{3+}$  doping content

$\text{CeO}_2:0.04\text{Sm}^{3+}, y\text{Eu}^{3+}$	FWHM	$2\theta^\circ$	$\text{Cos}(\theta)$	Crystal size (nm)
$y = 0.00$	0.005655	28.60	0.969016	25.3
$y = 0.02$	0.005498	28.58	0.969059	26.1
$y = 0.04$	0.005236	28.54	0.969145	27.3
$y = 0.06$	0.004992	28.52	0.969188	28.6
$y = 0.08$	0.004817	28.52	0.969209	29.7
$y = 0.10$	0.004643	28.50	0.969231	30.8

nanoparticles with an average size of approximately 40.5 nm (inset of Fig. 2a). Meanwhile, the doped sample ( $\text{CeO}_2:0.04\text{Sm}^{3+}, 0.04\text{Eu}^{3+}$ ) shows uniform grains, with boundary distribution and an average particle size of about 46.5 nm (inset of Fig. 2b). This finding suggests the high crystallinity of the obtained phosphors. However, the morphology of the samples did not significantly change, indicating that it is not a main parameter that can influence luminescent properties. Chemical element composition was analyzed using EDS to confirm the presence of ions doped into the  $\text{CeO}_2$  host. Fig. 2c shows the presence of Ce, O, and Sm, which are attributed to the host lattice and doping ion. Meanwhile, Fig. 2d indicates the presence of Ce, O, Eu, and Sm with percent composition shown in the inset of Fig. 2d. Impurity elements were not observed, thereby confirming the high purity of the obtained phosphors.

### 3.3. Luminescence properties

#### 3.3.1. Luminescence properties of $\text{CeO}_2:\text{Sm}$ and $\text{CeO}_2:\text{Sm}, \text{Eu}$ phosphors. Fig. 3a shows the photoluminescence excitation

(PLE) spectra of  $\text{CeO}_2:0.02\text{Sm}^{3+}$  with monitoring emission wavelengths of 573 and 615 nm. The absorption band from 250 nm to 300 nm is attributed to the charge transfer band from  $\text{O}^{2-}$  to  $\text{Ce}^{4+}$ . The highest band absorption with a peak at 360 nm corresponds to the overlap between the  ${}^6\text{H}_{5/2}-{}^4\text{D}_{3/2}$  transition of  $\text{Sm}^{3+}$  and the charge transfer band  $\text{O}^{2-}-\text{Ce}^{4+}/\text{Sm}^{3+}$ . The weak peak absorption at 405 nm corresponds to the  ${}^6\text{H}_{5/2}-{}^4\text{F}_{7/2}$  transition of  $\text{Sm}^{3+}$ . The band absorption with 573 nm emission is higher than that with 615 nm, indicating the dominant orange emission of the phosphors. Meanwhile, Fig. 3b presents the emission spectra of all investigated samples of  $\text{CeO}_2:x\text{Sm}^{3+}$  ( $x = 0.02, 0.04, 0.06, 0.08, 0.10,$  and  $0.12$  mol%) monitoring at excited wavelength of 360 nm. Under 360 nm excitation, the obtained phosphor showed characteristic emission of  $\text{Sm}^{3+}$ , such as at 573 ( ${}^4\text{G}_{5/2}-{}^6\text{H}_{5/2}$ ), 631 ( ${}^4\text{G}_{5/2}-{}^6\text{H}_{6/2}$ ), and 660 nm ( ${}^4\text{G}_{5/2}-{}^6\text{H}_{9/2}$ ). The emission intensity of the samples reached the maximum value of 0.04 mol%  $\text{Sm}^{3+}$  doping and then decreased with increasing  $\text{Sm}^{3+}$  content due to the concentration quenching effect. The sample  $\text{CeO}_2:0.04 \text{Sm}^{3+}$  showed the highest emission intensity and was selected for synthesis of  $\text{CeO}_2:0.04\text{Sm}^{3+}, y\text{Eu}^{3+}$  phosphor.

Fig. 4a presents the PLE spectra of samples  $\text{CeO}_2:0.04\text{Eu}^{3+}$  and  $\text{CeO}_2:0.04\text{Sm}^{3+}, 0.04\text{Eu}^{3+}$  with monitoring emission wavelength at 631 nm. In the typical two samples, the absorption bands from 250 nm to 300 are attributed to the charge transfer band from  $\text{O}^{2-}$  to  $\text{Ce}^{4+}$ , similar to the PLE spectra of  $\text{CeO}_2:0.04\text{Sm}^{3+}$ . The highest absorption band around at 360 nm corresponds to the overlap between the  ${}^6\text{H}_{5/2}-{}^4\text{D}_{3/2}$  transition of  $\text{Sm}^{3+}$  and the charge transfer band ( $\text{O}^{2-}$  to  $\text{Ce}^{4+}/\text{Sm}^{3+}/\text{Eu}^{3+}$ ) of the host lattice (sample  $\text{CeO}_2:0.04\text{Sm}^{3+}, 0.04\text{Eu}^{3+}$ ). Fig. 4a shows typical absorption peaks at 405 nm corresponding to the  ${}^6\text{H}_{5/2}$



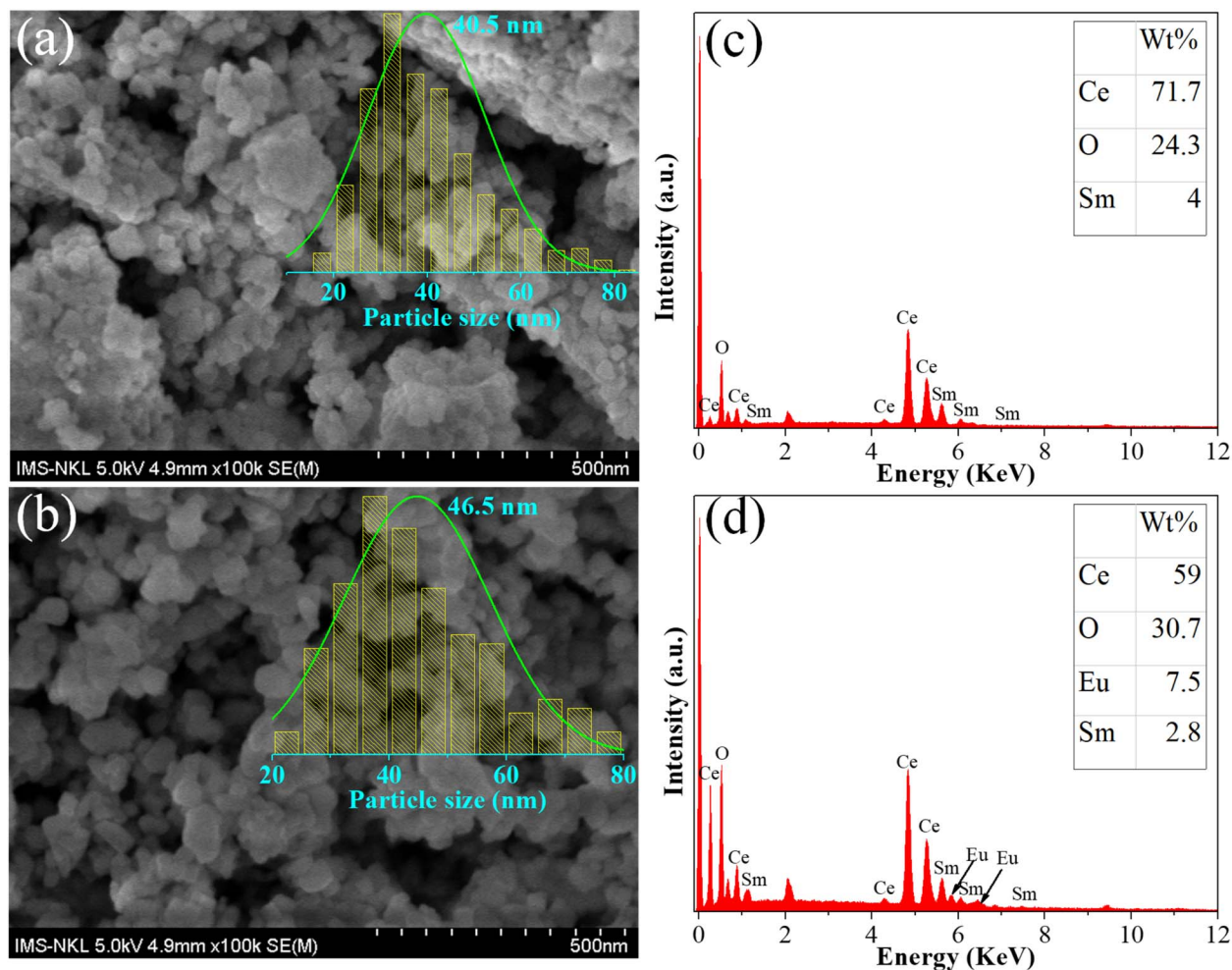


Fig. 2 SEM image of  $\text{CeO}_2:0.04\text{Sm}^{3+}$  (a) and  $\text{CeO}_2:0.04\text{Sm}^{3+}, 0.04\text{Eu}^{3+}$  (b); and EDS spectra of  $\text{CeO}_2:0.04\text{Sm}^{3+}$  (c) and  $\text{CeO}_2:0.04\text{Sm}^{3+}, 0.04\text{Eu}^{3+}$  (d).

$2-^4\text{F}_{7/2}$  transition of  $\text{Sm}^{3+}$ , while the absorption peak at 395 nm ( $^7\text{F}_0-^5\text{L}_6$ ), 466 nm ( $^7\text{F}_0-^5\text{D}_2$ ), 526/532 ( $^7\text{F}_0-^5\text{D}_1/^7\text{F}_1-^5\text{D}_1$ ) nm and 580/587 nm ( $^7\text{F}_0-^5\text{D}_0/^7\text{F}_1-^5\text{D}_0$ ) is attributed to the  $\text{Eu}^{3+}$ . These

results confirm the presence of dopant ions in the host lattice and the successful synthesis of the phosphors. In this case the absorption intensity from 250–400 nm of  $\text{CeO}_2:0.04\text{Sm}^{3+}$ ,

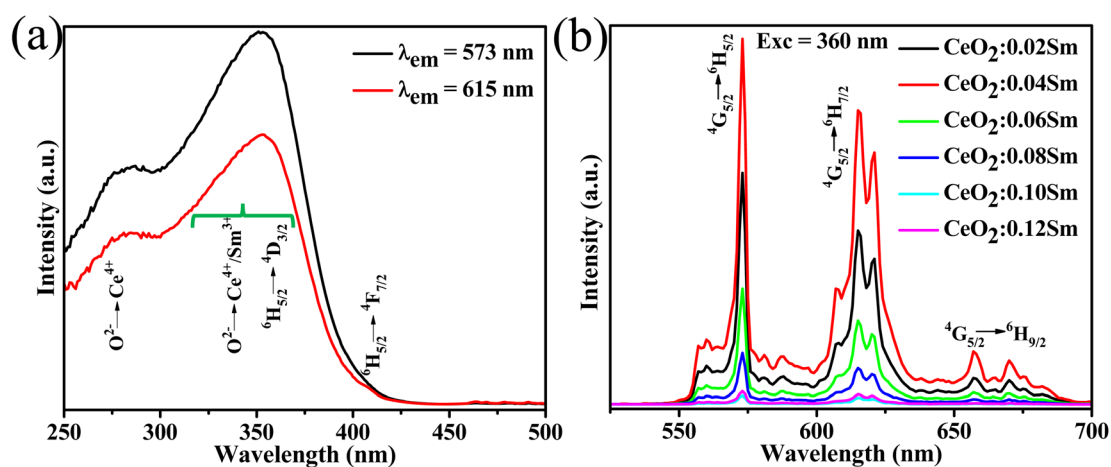


Fig. 3 (a) PLE spectra of  $\text{CeO}_2:0.04\text{Sm}^{3+}$  and (b) PL spectra of  $\text{CeO}_2:x\text{Sm}^{3+}$  ( $x = 0.02, 0.04, 0.06, 0.08, 0.10, \text{ and } 0.12$  mol%).



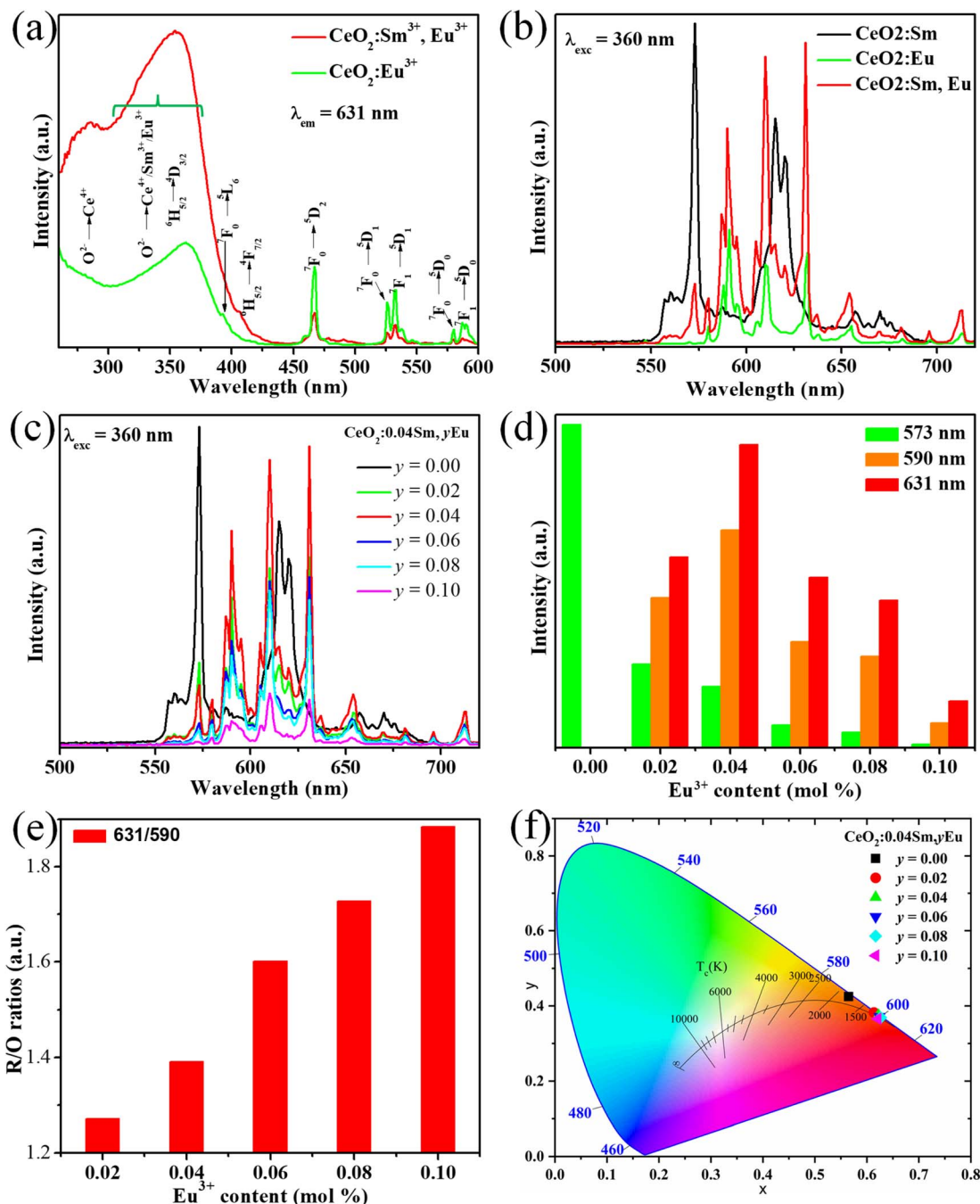


Fig. 4 (a) PLE spectra of samples  $\text{CeO}_2:0.04\text{Eu}^{3+}$  and  $\text{CeO}_2:0.04\text{Sm}^{3+}, 0.04\text{Eu}^{3+}$ ; (b) emission spectra of  $\text{CeO}_2:\text{Sm}^{3+}$ ,  $\text{CeO}_2:\text{Eu}^{3+}$ , and  $\text{CeO}_2:\text{Sm}^{3+}, \text{Eu}^{3+}$  phosphors; (c) PL emission spectra of samples  $\text{CeO}_2:0.04\text{Sm}^{3+}, y\text{Eu}^{3+}$  ( $y = 0.00, 0.02, 0.04, 0.06, 0.08,$  and  $0.10$ ); (d) dependence of the  ${}^4\text{G}_{5/2}-{}^6\text{H}_{5/2}$  ( $\text{Sm}^{3+}$ ) and  ${}^5\text{D}_0-{}^7\text{F}_1/{}^7\text{F}_2$  ( $\text{Eu}^{3+}$ ) transitions on the  $\text{Eu}^{3+}$  doping content; (e) red/orange (R/O) emission intensity ratios of investigated samples as  $\text{Eu}^{3+}$  content increased; (f) CIE coordinate chromaticity of  $\text{CeO}_2:0.04\text{Sm}^{3+}, y\text{Eu}^{3+}$  phosphors ( $y = 0.00, 0.02, 0.04, 0.06, 0.08,$  and  $0.10$ ).

$0.04\text{Eu}^{3+}$  was much higher than the  $\text{CeO}_2:0.04\text{Eu}^{3+}$ . Fig. 4b shows the difference in emission spectra between three phosphors ( $\text{CeO}_2:0.04\text{Sm}^{3+}$ ,  $\text{CeO}_2:0.04\text{Eu}^{3+}$  and  $\text{CeO}_2:0.04\text{Sm}^{3+}, 0.04\text{Eu}^{3+}$ ) under 360 nm excitation. Notably, the  $\text{CeO}_2:0.04\text{Sm}^{3+}$  phosphor emits a dominant peak of yellow light (573 nm), and the  $\text{CeO}_2:0.04\text{Eu}^{3+}$  phosphor emits an orange light (590 nm); however, the  $0.04\text{Sm}^{3+}/0.04\text{Eu}^{3+}$  co-doped  $\text{CeO}_2$  exhibited a dominant peak red emission (631 nm). The

photoluminescence spectra of all investigated samples are shown in Fig. 4c. Under 360 nm excitation wavelengths, the  $\text{CeO}_2:0.04\text{Sm}^{3+}, y\text{Eu}^{3+}$  ( $y = 0, 0.02, 0.04, 0.06, 0.08,$  and  $0.10$ ) phosphors emitted strong orange-red band at 590 nm ( ${}^5\text{D}_0-{}^7\text{F}_1$ ) and 610–631 nm ( ${}^5\text{D}_0-{}^7\text{F}_2$ ) of  $\text{Eu}^{3+}$ . Notably, the emission intensities at 573 nm corresponding to the  ${}^4\text{G}_{5/2}-{}^6\text{H}_{5/2}$  transition of  $\text{Sm}^{3+}$  decreased with increasing  $\text{Eu}^{3+}$  doping content. By contrast, the emission intensities at 631 nm depended on  $\text{Eu}^{3+}$



Table 2 CIE chromaticity coordinates, color purity, and CCT values of all investigated samples

Samples	Chromaticity coordinates (x, y)	Color purity (%)	CCT (K)
CeO <sub>2</sub> :0.04Sm	(0.565, 0.425)	77.60	1847
CeO <sub>2</sub> :0.04Sm, 0.02Eu	(0.614, 0.383)	86.93	1790.8
CeO <sub>2</sub> :0.04Sm, 0.04Eu	(0.622, 0.375)	88.95	1885.8
CeO <sub>2</sub> :0.04Sm, 0.06Eu	(0.624, 0.371)	89.36	1936.2
CeO <sub>2</sub> :0.04Sm, 0.08Eu	(0.626, 0.370)	89.74	1974.8
CeO <sub>2</sub> :0.04Sm, 0.10Eu	(0.621, 0.366)	88.10	1973.1

content and reached the maximum value at 0.04 mol% Eu<sup>3+</sup> doping (Fig. 4d). Hence, the red-emitting phosphors (CeO<sub>2</sub>:0.04Sm<sup>3+</sup>, 0.04Eu<sup>3+</sup>) could be excited by 360 nm commercial LED chip, making it suitable for solid lighting applications. Furthermore, the red/orange (R/O) emission intensity ratios of the CeO<sub>2</sub>:0.04Sm<sup>3+</sup>, yEu<sup>3+</sup> (y = 0, 0.02, 0.04, 0.06, 0.08, and 0.10) phosphors can estimate the asymmetry around the Eu<sup>3+</sup> sites in the host lattice,<sup>29</sup> which was calculated as shown in Fig. 4e. The R/O ratio increases with the enhancement of Eu<sup>3+</sup> content, confirming the asymmetry of the crystal field increased. These results supported increasing the electric-dipole transition probability of the Eu<sup>3+</sup>, resulting in dominant red emissions. In addition, the Commission Internationale de l'Eclairage (CIE) chromaticity coordinates of resulted phosphors (Fig. 4f) were calculated from their emission spectra, as shown in Table 2. CeO<sub>2</sub>:0.04Sm<sup>3+</sup>, 0.04Eu<sup>3+</sup> shows CIE coordinates (0.622, 0.375) close to pure red.<sup>14</sup> Furthermore, these CIE coordinates were used for calculating the color purity of the investigated phosphors, which can be described as eqn (2):<sup>30</sup>

$$\text{Color purity} = \frac{\sqrt{(x - x_i)^2 + (y - y_i)^2}}{\sqrt{(x_d - x_i)^2 + (y_d - y_i)^2}} \times 100\% \quad (2)$$

where (x, y) and (x<sub>i</sub> = 0.3333, y<sub>i</sub> = 0.3333) are the color coordinates of the investigated samples and the white light source, respectively; (x<sub>d</sub>, y<sub>d</sub>) corresponds to the color coordinates of the dominant wavelength.<sup>31</sup> These values (x, y), (x<sub>i</sub>, y<sub>i</sub>), and (x<sub>d</sub>, y<sub>d</sub>) were plugged into eqn (2), and the color purity of the resulting

phosphors is displayed in Table 2. The color purity of the samples increased with enhancing Eu<sup>3+</sup> doping content and reached a maximum value of 89.74% (Table 2). The findings confirm the high efficiency ET from Sm<sup>3+</sup> to Eu<sup>3+</sup> in the systems developed. Furthermore, the correlation of phosphors with color temperature (CCT) was calculated to explore the nature of the emitted light by using McCammys' equation:<sup>32</sup>

$$\text{CCT} = 5520.33 - 6823n + 3525n^2 - 449n^3 \quad (3)$$

where (x, y) is the CIE coordinates of all samples; (x<sub>e</sub> = 0.338, y<sub>e</sub> = 0.186) is the chromaticity epicenter; n = (x - x<sub>e</sub>)/(y - y<sub>e</sub>). The resulting CCT values are shown in Table 2. The values increased from 1790.8 K to 1973 K with increasing Eu<sup>3+</sup> doping content.

**3.3.2. Decay curves and ET efficiency of all obtained phosphors.** The decay curve of Sm<sup>3+</sup> in CeO<sub>2</sub>:0.04Sm<sup>3+</sup>, yEu<sup>3+</sup>

Table 3 Fitting decay curves for CeO<sub>2</sub>:0.04Sm<sup>3+</sup>, xEu<sup>3+</sup> (x = 0, 0.02, 0.04, 0.06, 0.08 and 0.10 mol%)

CeO <sub>2</sub> :0.04Sm, yEu	A <sub>1</sub>	τ <sub>1</sub>	A <sub>2</sub>	τ <sub>2</sub>	τ <sub>average</sub> (ms)
y = 0.00	82.25	1.11	227	0.23	1.701
y = 0.02	319.7	1.12	926	0.23	0.788
y = 0.04	932	0.21	260	0.99	0.653
y = 0.06	131	0.7	743	0.17	0.512
y = 0.08	166.9	0.85	746	0.2	0.319
y = 0.10	653.6	0.15	76.76	0.62	0.309

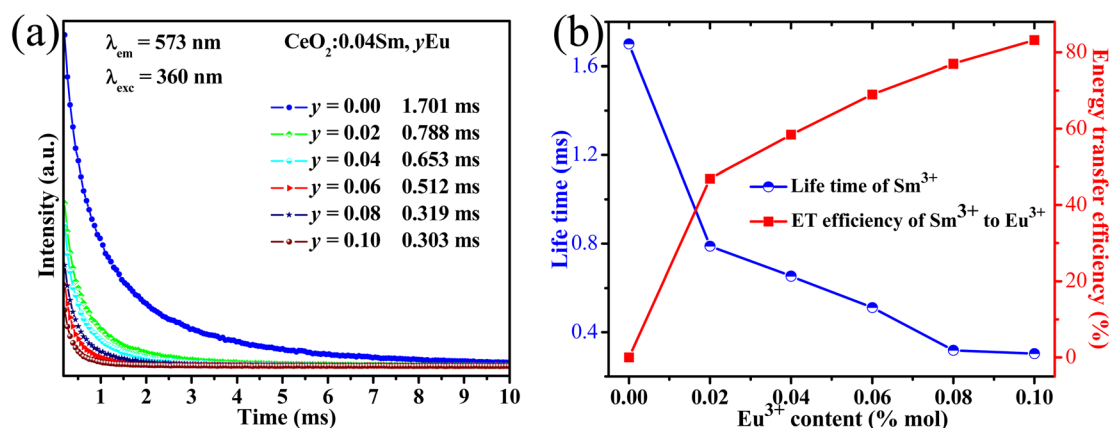


Fig. 5 (a) Decay curve of samples monitored at the excitation wavelength of 360 nm and the emission wavelength of 573 nm. (b) Lifetime of all sample depended on Eu<sup>3+</sup> content (blue line) and ET efficiency from Sm<sup>3+</sup> to Eu<sup>3+</sup> (red line).



Table 4 Comparison of ET efficiency from Sm<sup>3+</sup> to Eu<sup>3+</sup> on the proposed phosphor and other existing phosphors

Phosphors	Content of Eu <sup>3+</sup> (mol%)	ET efficiency (%)	References
CeO <sub>2</sub> :Sm <sup>3+</sup> , Eu <sup>3+</sup>	0.04	84.00	This work
La <sub>2</sub> MgTiO <sub>6</sub> :Sm <sup>3+</sup> , Eu <sup>3+</sup>	0.20	73.50	35
YPO <sub>4</sub> :Sm <sup>3+</sup> , Eu <sup>3+</sup>	0.08	65.00	16
Ca <sub>2</sub> GdNbO <sub>6</sub> :Sm <sup>3+</sup> , Eu <sup>3+</sup>	0.30	28.60	12
Sr <sub>7</sub> Sb <sub>2</sub> O <sub>12</sub> :Sm <sup>3+</sup> , Eu <sup>3+</sup>	0.09	42.40	7
Sr <sub>3</sub> In <sub>2</sub> WO <sub>6</sub> :Sm <sup>3+</sup> , Eu <sup>3+</sup>	0.02	62.69	18
Sr <sub>3</sub> Y(BO <sub>3</sub> ) <sub>3</sub> :Sm <sup>3+</sup> , Eu <sup>3+</sup>	0.07	55.69	33

phosphor ( $y = 0.00, 0.02, 0.04, 0.06, 0.08,$  and  $0.10$ ) can be used to study the emission mechanism and confirm the efficiency of ET from Sm<sup>3+</sup> to Eu<sup>3+</sup>. The luminescence decay curves associated with the transition  ${}^4G_{5/2} - {}^6H_{5/2}$  of Sm<sup>3+</sup> of all samples were monitored at the emission wavelength of 573 nm and the excitation wavelength of 360 nm (Fig. 5a). The radiative lifetime ( $\tau$ ) of the samples well fitted by bi-exponential function:<sup>33</sup>

$$y = y_0 + A_1 e^{-t/\tau_1} + A_2 e^{-t/\tau_2} \quad (4)$$

where  $y$  is the emission intensity at time  $t$ ;  $y_0$  is the initial emission intensity;  $A_1$  and  $A_2$  are constants;  $\tau_1$  and  $\tau_2$  are decay times.  $\tau_1$  is the decay component attributed to Sm<sup>3+</sup> on the surface or near defect sites. By contrast,  $\tau_2$  is the decay component associated with Sm<sup>3+</sup> sites substituted for Ce<sup>4+</sup> ions on the CeO<sub>2</sub> host lattice.<sup>33</sup> The average lifetimes ( $\tau$ ) can be described as eqn (5):<sup>34</sup>

$$\tau = \frac{A_1 \tau_1^2 + A_2 \tau_2^2}{A_1 \tau_1 + A_2 \tau_2} \quad (5)$$

The  $\tau$  values are 1.701, 0.788, 0.653, 0.512, 0.319, and 0.303 ms, corresponding to CeO<sub>2</sub>:0.04Sm<sup>3+</sup>,  $y$ Eu<sup>3+</sup> phosphors ( $y = 0, 0.02, 0.04, 0.06, 0.08,$  and  $0.10$  mol%, respectively), as shown in Table 3. The average lifetime decreased with increasing Eu<sup>3+</sup> doping content, thereby confirming the ET from Sm<sup>3+</sup> to Eu<sup>3+</sup>.<sup>12,35</sup> Furthermore, ET efficiency was estimated using eqn (6):<sup>36</sup>

$$\eta_T = 1 - \frac{\tau_S}{\tau_{S0}} \quad (6)$$

where  $\tau_S$  and  $\tau_{S0}$  are the lifetimes of Sm<sup>3+</sup> with and without Eu<sup>3+</sup>, respectively. The calculated ET efficiency values are shown in Fig. 5b. The ET efficiency from Sm<sup>3+</sup> to Eu<sup>3+</sup> increased with increasing doping content of Eu<sup>3+</sup> and reached the maximum value of 84% with 0.10 mol% Eu<sup>3+</sup>. The ET efficiency in this work is significantly higher than in other previous works (Table 4). These results indicated that the phosphor conferred it as a suitable red-emitting phosphor for WLEDs.

**3.3.3. ET mechanism.** The exchange interaction or multipolar interaction is responsible for the main ET mechanism in the CeO<sub>2</sub>:Sm<sup>3+</sup>, Eu<sup>3+</sup>, which is estimated by the average critical

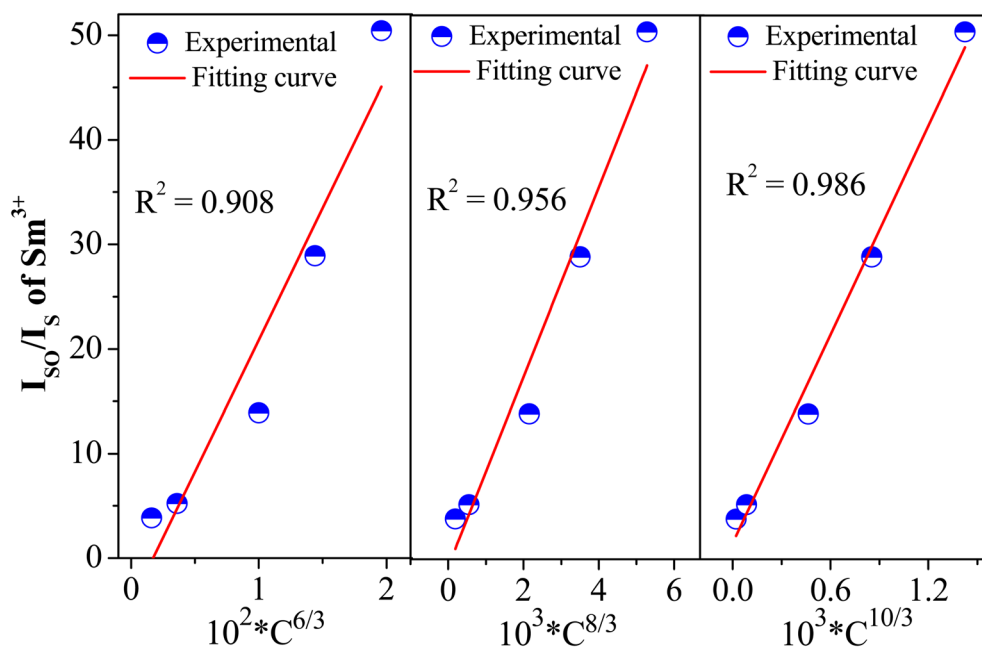


Fig. 6 Dependence of the  $I_{50}/I_5$  intensity ratio of Sm<sup>3+</sup> on  $C^{6/3}$ ,  $C^{8/3}$ , and  $C^{10/3}$  in CeO<sub>2</sub>:0.04Sm<sup>3+</sup>,  $y$ Eu<sup>3+</sup> phosphors ( $y = 0.00, 0.02, 0.04, 0.06, 0.08,$  and  $0.10$ ).



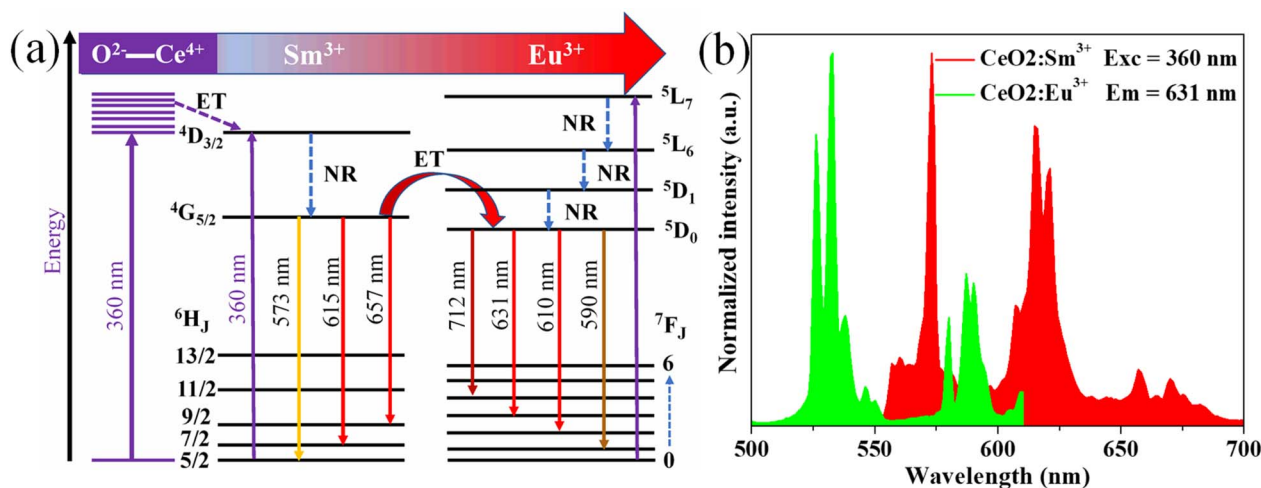


Fig. 7 (a) Schematic energy-level diagram of  $\text{CeO}_2:0.04\text{Sm}^{3+}, y\text{Eu}^{3+}$  phosphors with excitation, emission, and energy transfer; (b) the overlap between the excitation spectra of sample  $\text{CeO}_2:0.04\text{Eu}^{3+}$  and the emission spectra of sample  $\text{CeO}_2:0.04\text{Sm}^{3+}$ .

distance ( $R_C$ ) between  $\text{Sm}^{3+}$  and  $\text{Eu}^{3+}$ . Notably, the multipolar interaction is attributed to the  $R_C$  value higher 5 Å and when the  $R_C$  is about 5 Å corresponding to exchange interaction.<sup>37</sup> The  $R_C$  value can be determined by eqn (7):<sup>37</sup>

$$R_C = \left[ \frac{6V}{\pi\chi_C N} \right]^{1/3} \quad (7)$$

here, the cell volume  $V$  is  $430.32 \text{ \AA}^3$ ; the critical doping content  $\chi_C$  is 0.08;  $N$  is the available host cations in the cell.<sup>38</sup> Putting all these values in the eqn (7), the  $R_C$  value in  $\text{CeO}_2:0.04\text{Sm}^{3+}, 0.04\text{Eu}^{3+}$  was observed to be  $\sim 13.7 \text{ \AA}$ , thus, the ET mechanism from  $\text{Sm}^{3+}$  to  $\text{Eu}^{3+}$  occurs by multipolar interaction. In this case, the Dexter theory was explored to evaluate the multipolar interaction between  $\text{Sm}^{3+}$  and  $\text{Eu}^{3+}$ .<sup>39</sup> Therefore, the rate of ET from  $\text{Sm}^{3+}$  to  $\text{Eu}^{3+}$  against the concentration of  $\text{Eu}^{3+}$  can be estimated as follows:<sup>39</sup>

$$\frac{I_{S0}}{I_S} \propto C^{n/3} \quad (8)$$

where  $C$  is the total doping ion content ( $\text{Sm}^{3+}$  and  $\text{Eu}^{3+}$ ).  $I_{S0}$  and  $I_S$  are the emission intensity of  $\text{Sm}^{3+}$  without and with  $\text{Eu}^{3+}$  doping. The  $n$  is an electric multipolar character equal to 6, 8, and 10, corresponding to dipole–dipole, dipole–quadrupole, and quadrupole–quadrupole interactions.<sup>11</sup> Fig. 6 shows the relationship between  $C^{n/3}$  and  $I_{S0}/I_S$ , including the values of the fitting factor  $R^2$ . Previous works<sup>18,33,35,40</sup> indicate that the  $R^2$  highest value (close to 1) determines the ET mechanism in the system. Therefore, the  $R^2$  highest value in this work is 0.986, indicating the ET mechanism in  $\text{CeO}_2:\text{Sm}^{3+}, \text{Eu}^{3+}$  corresponding to quadrupole–quadrupole interaction.

**3.3.4. Energy level diagram of the phosphors.** Furthermore, the ET process from  $\text{Sm}^{3+}$  to  $\text{Eu}^{3+}$  can be explained using an energy level diagram (Fig. 7a). Under 360 nm wavelength excitation, the electron at the  ${}^6\text{H}_{5/2}$  state of  $\text{Sm}^{3+}$  absorption photons move to the  ${}^4\text{D}_{3/2}$  level. In addition, the population of the  ${}^4\text{D}_{3/2}$  level is enhanced by absorption due to the charge transfer from  $\text{O}^{2-}$  to  $\text{Ce}^{4+}$  of the host lattice. The electrons in the

${}^4\text{D}_{3/2}$  level relax to the  ${}^4\text{G}_{5/2}$  state through non-radiation transition. Finally, the electrons at the  ${}^4\text{G}_{5/2}$  of  $\text{Sm}^{3+}$  transfer energy to the  ${}^5\text{D}_0$  state of  $\text{Eu}^{3+}$  and then go back to the ground state  ${}^7\text{F}_j$  ( $j = 0, 1, 2$ , and 4), thereby producing intense red emission band. The ET was confirmed by the spectral overlap between the excitation of  $\text{Eu}^{3+}$  and the emission of  $\text{Sm}^{3+}$ , as shown in Fig. 7b.

## 4. Conclusion

$\text{CeO}_2:\text{Sm}^{3+}$  and  $\text{CeO}_2:\text{Sm}^{3+}, \text{Eu}^{3+}$  phosphors were successfully synthesized using solution combustion. The XRD analysis confirmed the formation of single-phase cubic  $\text{CeO}_2$  with space group  $Fm\bar{3}m$ . Under 360 nm excitation,  $\text{CeO}_2:\text{Sm}^{3+}$  phosphors emitted strong yellow-red band at 573 and 615 nm, corresponding to the  ${}^4\text{G}_{5/2}-{}^6\text{H}_j$  ( $j = 5/2$ , and  $6/2$ ) transitions of  $\text{Sm}^{3+}$ . Meanwhile,  $\text{CeO}_2:\text{Sm}^{3+}, \text{Eu}^{3+}$  showed the emission characteristics of  $\text{Sm}^{3+}$  (573 nm) and  $\text{Eu}^{3+}$  at 590/610–631 nm. The photoluminescence spectra showed the ET from  $\text{Sm}^{3+}$  to  $\text{Eu}^{3+}$  because of the small energy difference between the  ${}^4\text{G}_{5/2}$  level of  $\text{Sm}^{3+}$  and the  ${}^5\text{D}_0$  level of  $\text{Eu}^{3+}$  ions. Significantly, the decay kinetics of the  ${}^4\text{G}_{5/2}-{}^6\text{H}_{5/2}$  transition ( $\text{Sm}^{3+}$ ) in  $\text{CeO}_2:\text{Sm}^{3+}, \text{Eu}^{3+}$  confirmed the high-efficiency ET from  $\text{Sm}^{3+}$  to  $\text{Eu}^{3+}$  (up to 84%). The quadrupole–quadrupole interaction between  $\text{Sm}^{3+}$  and  $\text{Eu}^{3+}$  was responsible for the ET mechanism. These results indicate that the high-efficiency ET from  $\text{Sm}^{3+}$  to  $\text{Eu}^{3+}$  in  $\text{CeO}_2:\text{Sm}^{3+}, \text{Eu}^{3+}$  phosphors are an excellent strategy to improve the emission efficiency of  $\text{Eu}^{3+}$ .

## Author contributions

Nguyen Van Hai: data curation, format analysis, resources, supervision, writing – original draft. Bui Thi Hoan: investigation, data curation. Nguyen Minh Tu: conceptualization, format analysis. Dinh Thi Hien: methodology, resources. Nguyen Thi Khanh Linh: format analysis, experiment, methodology, data curation. Duy-Hung Nguyen: methodology, data curation. Vu Tuan Anh: format analysis, experiment. Vuong-Hung Pham:





format analysis, conceptualization. Hoang Nhu Van: investigation, format analysis, experiment, conceptualization, methodology, writing – original draft, writing – review & editing.

## Conflicts of interest

The authors declare that they have no conflict of interest.

## Acknowledgements

This work is funded by the Ministry of Education and Training of Vietnam, under the project B2023-SPH-06.

## References

- 1 S. Wang, Z. Song and Q. Liu, Recent progress in  $\text{Ce}^{3+}/\text{Eu}^{2+}$ -activated LEDs and persistent phosphors: focusing on the local structure and the electronic structure, *J. Mater. Chem. C*, 2023, **11**, 48–96.
- 2 M. Iwaki, K. Uematsu, M. Sato and K. Toda, Structure and Luminescence Studies of a  $\text{Ce}^{3+}$ -Activated  $\text{Ba}_5\text{La}_3\text{MgAl}_3\text{O}_{15}$  Green-Emitting Phosphor, *Inorg. Chem.*, 2023, **62**, 1250–1256.
- 3 P. Dang, D. Liu, G. Li, A. A. Al Kheraif and J. Lin, Recent Advances in Bismuth Ion-Doped Phosphor Materials: Structure Design, Tunable Photoluminescence Properties, and Application in White LEDs, *Adv. Opt. Mater.*, 2020, **8**, 1901993.
- 4 T. K. Kuttiat, M. Abraham, A. K. Kunti, N. Amador-Mendez, M. Tchernycheva and S. Das, Enriching the Deep-Red Emission in  $(\text{Mg}, \text{Ba})_3\text{M}_2\text{GeO}_8$ :  $\text{Mn}^{4+}$  ( $\text{M} = \text{Al}, \text{Ga}$ ) Compositions for Light-Emitting Diodes, *ACS Appl. Mater. Interfaces*, 2023, **15**, 7083–7101.
- 5 T. Zhuang, Y. Lin, J. Jin, Z. Deng, Y. Peng, L. Gong, Z. Wang, K. Du and X. Huang, A Mechanochemically Synthesized Hybrid Bismuth Halide as Highly Efficient Red Phosphor for Blue Chip-Based WLED, *Adv. Opt. Mater.*, 2023, **11**, 2202951.
- 6 G. Wu, J. Xue, X. Li, Q. Bi, M. Sheng and Z. Leng, A novel red-emitting  $\text{Na}_5\text{W}_3\text{O}_9\text{F}_5$ : $\text{Eu}^{3+}$  phosphor with high color purity for blue-based WLEDs, *Ceram. Int.*, 2023, **49**, 10615–10624.
- 7 S. Ling, F. B. Xiong, W. B. Yang, H. F. Lin and W. Z. Zhu, Novel  $\text{Sm}^{3+}/\text{Eu}^{3+}$  co-doped  $\text{Sr}_7\text{Sb}_2\text{O}_{12}$  red-emitting phosphor for white LED, *Inorg. Chem. Commun.*, 2022, **150**, 110365.
- 8 H. N. Van, P. D. Tam and V. H. Pham, Red and Yellow Luminescence of  $\text{Eu}^{3+}/\text{Dy}^{3+}$  Co-Doped Hydroxyapatite/ $\beta$ -Tricalcium Phosphate Single Phosphors Synthesized Using Coprecipitation Method, *J. Appl. Spectrosc.*, 2018, **85**, 738–742.
- 9 H. N. Van, M. T. Y. Thanh, P. H. Vuong, P. V. Huan, V. T. N. Minh, P. A. Tuan and T. D. Hien, Experimental and theoretical studies of red emission enhancing mechanism in Al-doped  $\text{CaMoO}_4$ :Eu phosphor, *Opt. Mater.*, 2022, **132**, 112831.
- 10 P. V. Huan, B. T. Hue, B. T. Hoan, N. T. H. Thanh, H. N. Van, C. X. Thang, H. H. Anh, P. D. Tam and P. H. Vuong, Correlation of luminescence and Judd-Ofelt intensity parameters in red  $\text{ZrO}_2$ :  $\text{Eu}^{3+}$ ,  $\text{Al}^{3+}$  phosphor: the influences of  $\text{Al}^{3+}$  ions, *Mater. Sci. Eng. B: Solid-State Mater. Adv. Technol.*, 2020, **32**, 114794.
- 11 S. Sharma, A. S. Rao and K. Kishore, Energy transfer dynamics in thermally stable  $\text{Sm}^{3+}/\text{Eu}^{3+}$  co-doped AEALBS glasses for near UV triggered photonic device applications, *J. Non-Cryst. Solids*, 2021, **580**, 121392.
- 12 X. Zhang, R. Cui, K. Guo, M. Zhang, J. Zhang and C. Deng, Luminescence properties of  $\text{Ca}_2\text{GdNbO}_6$ :  $\text{Sm}^{3+}$ ,  $\text{Eu}^{3+}$  red phosphors with high quantum yield and excellent thermal stability for WLEDs, *Ceram. Int.*, 2023, **49**, 15402–15412.
- 13 P. K. Pandey, P. Dixit, V. Chauhan and P. C. Pandey, Luminescence properties and energy transfer studies in thermally stable  $\text{Bi}_2\text{O}_3$ :  $\text{Sm}^{3+}$ ,  $\text{Eu}^{3+}$  phosphor, *J. Alloys Compd.*, 2023, **952**, 169911.
- 14 E. Rai, A. Roy, A. Rai, V. J. Fulari and S. B. Rai, Structural and luminescent properties and energy transfer from  $\text{Tb}^{3+}$  to  $\text{Eu}^{3+}$  in  $\text{LaVO}_4$ : $x\text{Tb}^{3+}/y\text{Eu}^{3+}$  phosphors, *J. Alloys Compd.*, 2023, **937**, 168395.
- 15 X. Wu, X. Zhao, Q. Ren, L. Du, M. Pei and O. Hai, Design efficient energy transfer  $\text{Ca}_2\text{Al}_2\text{SiO}_7$ :  $\text{Bi}^{3+}$ ,  $\text{Eu}^{3+}$  phosphors by cationic substitution for full-spectrum W-LED lighting, *Ceram. Interfaces*, 2023, **49**, 18852–18860.
- 16 J. Wu, C. Liu, H. Jia, Y. Qi, Z. Liu, Y. Hu and F. Feng, Optical properties, energy transfer and thermal stability of spherical nano-phosphor  $\text{YPO}_4$ : $\text{Eu}^{3+}$ : $\text{Sm}^{3+}$ , *J. Lumin.*, 2022, **245**, 118791.
- 17 Y. Li, X. Zhang, Y. Wang, S. Ma, F. Jing, Z. Hu and Y. Wu, Growth and optical properties of a  $\text{Sm}^{3+}$ ,  $\text{Eu}^{3+}$  co-doped  $\text{La}_2\text{CaB}_{10}\text{O}_{19}$  crystal, *J. Cryst. Growth*, 2023, **614**, 127243.
- 18 P. Yu, R. Cui, C. Xu, G. Zhang, J. Zhang and C. Deng, A novel efficient  $\text{Sr}_3\text{In}_2\text{WO}_9$ :  $\text{Sm}^{3+}$ ,  $\text{Eu}^{3+}$  phosphor for white LED applications, *Opt. Laser Technol.*, 2022, **163**, 109389.
- 19 L. Li, H. K. Yang, B. K. Moon, Z. Fu, C. Guo, J. H. Jeong, S. S. Yi, K. Jang and H. S. Lee, Photoluminescence Properties of  $\text{CeO}_2$ : $\text{Eu}^{3+}$  Nanoparticles Synthesized by a Sol-Gel Method, *J. Phys. Chem. C*, 2009, **113**, 610–617.
- 20 A. K. Pal, S. Som and C. H. Lu, Synthesis and spectroscopic analysis of  $\text{Sm}^{3+}$  doped  $\text{CeO}_2$  ceramic powders for the application of white LEDs, *Ceram. Int.*, 2018, **44**, 18256–18263.
- 21 N. V. Hai, D. T. Hien, N. T. K. Linh, B. T. Hoan, N. M. Tu and H. N. Van, Blue-excited red emission of  $\text{CeO}_2$ : $\text{Eu}^{3+}$ ,  $\text{Al}^{3+}$  cubic phosphor: influence of  $\text{Al}^{3+}$  ion doping and Judd-Ofelt theory, *J. Lumin.*, 2023, **263**, 120047.
- 22 C. R. Michel and A. H. Martínez-Preciado, CO sensor based on thick films of 3D hierarchical  $\text{CeO}_2$  architectures, *Sens. Actuators, B*, 2014, **197**, 177–184.
- 23 G. Vimal, K. P. Mani, D. Alexander, P. R. Biju, N. V. Unnikrishnan, M. A. Ittyachen and C. Joseph, Facile synthesis of  $\text{Sm}^{3+}/\text{Eu}^{3+}$  codoped  $\text{CeO}_2$  ultrafine nanocrystals and oxygen vacancy site dependent photoluminescence, *Opt. Mater.*, 2015, **50**, 220–228.
- 24 L. Sun, Y. Tan, D. Li, H. Du and D. Guo, Defects and symmetry influence on visible emission of  $\text{Bi}^{3+}$  co-doped  $\text{CeO}_2$ : $\text{Eu}^{3+}$  phosphor, *Opt. Mater.*, 2019, **100**, 109654.



- 25 K. Y. Jung, J. C. Lee, D. S. Kim, B. K. Choi and W. J. Kang, Co-doping effect of monovalent alkali metals on optical properties of CeO<sub>2</sub>:Eu nanophosphor prepared by spray pyrolysis and application for preparing pearlescent pigments with red emission, *J. Lumin.*, 2017, **192**, 1313–1321.
- 26 S. Mahamuda, K. Swapna, M. Venkateswarlu, A. S. Rao, S. Shakya and G. V. Prakash, Spectral characterisation of Sm<sup>3+</sup> ions doped oxy-fluoroborate glasses for visible orange luminescent applications, *J. Lumin.*, 2014, **154**, 410–424.
- 27 D. T. T. Dung, V. T. N. Minh, N. X. Truong, P. V. Huan, P. H. Vuong, N. D. Hung, B. T. Hoan, L. M. Tu and H. N. Van, Dual-mode green emission and temperature sensing properties of rare-earth-element-doped biphasic calcium phosphate composites, *J. Alloys Compd.*, 2021, **871**, 159483.
- 28 G. Ouertani, M. Ferhi, K. Horchani-Naifer and M. Ferid, Effect of Sm<sup>3+</sup> concentration and excitation wavelength on spectroscopic properties of GdPO<sub>4</sub>:Sm<sup>3+</sup> phosphor, *J. Alloys Compd.*, 2021, **885**, 161178.
- 29 U. Rambabu and S. Han, Luminescence optimization with superior asymmetric ratio (red/orange) and color purity of MBO<sub>3</sub>:Eu<sup>3+</sup>@SiO<sub>2</sub> (M = Y, Gd and Al) nano down-conversion phosphors, *RSC Adv.*, 2013, **3**, 1368–1379.
- 30 H. T. Nam, P. D. Tam, N. V. Hai and H. N. Van, Multifunctional optical thermometry using dual-mode green emission of CaZrO<sub>3</sub>:Er/Yb/Mo perovskite phosphors, *RSC Adv.*, 2023, **13**, 14660–14674.
- 31 P. Singh, H. Mishra, P. C. Pandey and S. B. Rai, Structure, photoluminescence properties, and energy transfer phenomenon in Sm<sup>3+</sup>/Eu<sup>3+</sup> co-doped CaTiO<sub>3</sub> phosphors, *New J. Chem.*, 2022, **47**, 1460–1471.
- 32 H. Duan, R. Cui, M. Zhang and C. Deng, Photoluminescence properties and energy transfer studies of Ba<sub>2</sub>YAlO<sub>5</sub>: Sm<sup>3+</sup>, Eu<sup>3+</sup> orange-red phosphors, *Optik*, 2021, **238**, 166774.
- 33 J. Zheng, X. Wu, Q. Ren, W. Bai, Y. Ren, M. Wang and O. Hai, Investigation of luminescence properties and energy transfer in Sm<sup>3+</sup> and Eu<sup>3+</sup> co-doped Sr<sub>3</sub>Y(BO<sub>3</sub>)<sub>3</sub> red phosphors, *Opt. Laser Technol.*, 2019, **122**, 105857.
- 34 H. Tang, X. Zhang, L. Cheng, L. Jiang, X. Mi, Q. Liu, J. Xie and Y. Wang, Photoluminescence properties and energy transfer mechanisms of Na<sub>4</sub>CaSi<sub>3</sub>O<sub>9</sub>: Sm<sup>3+</sup>, Eu<sup>3+</sup> novel orange-red phosphors, *J. Lumin.*, 2019, **214**, 116532.
- 35 B. Su, H. Xie, Y. Tan, Y. Zhao, Q. Yang and S. Zhang, Luminescent properties, energy transfer, and thermal stability of double perovskites La<sub>2</sub>MgTiO<sub>6</sub>:Sm<sup>3+</sup>, Eu<sup>3+</sup>, *J. Lumin.*, 2018, **204**, 457–463.
- 36 D. Geng, M. Shang, D. Yang, Y. Zhang, Z. Cheng and J. Lin, Tunable luminescence and energy transfer properties in KCaGd(PO<sub>4</sub>)<sub>2</sub>:Ln<sup>3+</sup>/Mn<sup>2+</sup> (Ln = Tb, Dy, Eu, Tm; Ce, Tb/Dy) phosphors with high quantum efficiencies, *J. Mater. Chem.*, 2012, **22**, 23789.
- 37 M. Shang, G. Li, X. Kang, D. Yang, D. Geng and J. Lin, Tunable Luminescence and Energy Transfer Properties of Sr<sub>3</sub>AlO<sub>4</sub>F:RE<sup>3+</sup> (RE = Tm/Tb, Eu, Ce) Phosphors, *ACS Appl. Mater. Interfaces*, 2011, **7**, 2738–2746.
- 38 R. B. Basavaraja, D. Navami, N. H. Deepthi, M. Venkataravanappa, R. Lokesh, K. H. S. Kumar and T. K. Sreelakshmi, Novel orange-red emitting Pr<sup>3+</sup> doped CeO<sub>2</sub> nanopowders for white light emitting diode applications, *Inorg. Chem. Commun.*, 2020, **120**, 108164.
- 39 E. F. Huerta, O. S. Romero, A. N. Meza-Rocha, S. Bordignon, A. Speghini and U. Caldino, Lithium-aluminum-zinc phosphate glasses activated with Sm<sup>3+</sup>, Sm<sup>3+</sup>/Eu<sup>3+</sup> and Sm<sup>3+</sup>/Tb<sup>3+</sup> for reddish-orange and white light generation, *J. Alloys Compd.*, 2020, **846**, 156332.
- 40 Q. Ren, B. Wang, X. Wu, T. Wei and Z. Huo, Luminescence properties and energy transfer in Dy<sup>3+</sup> and Eu<sup>3+</sup> co-doped Sr<sub>3</sub>Y(PO<sub>4</sub>)<sub>3</sub> phosphor, *J. Alloys Compd.*, 2016, **684**, 677–682.

